Available online at www.sciencedirect.com
SCIENCE DIRECT®
Electrochemistry Communications 7 (2005) 781–788
electrochemistry communications
www.elsevier.com/locate/elecom

Electrochemical study of ferrocene intercalated vanadium pentoxide xerogel/polyvinyl alcohol composite films: Application in the development of amperometric biosensors

Constantinos G. Tsiafoulis [a], Ageliki B. Florou [a], Pantelis N. Trikalitis [b], Thomas Bakas [c], Mamas I. Prodromidis [a,*]

[a] Department of Chemistry, Laboratory of Analytical Chemistry, University of Ioannina, 45110 Ioannina, Greece
[b] Department of Chemistry, University of Crete, 71409 Heraklion Crete, Greece
[c] Department of Physics, University of Ioannina, 45110 Ioannina, Greece

Received 7 April 2005; received in revised form 25 April 2005; accepted 25 April 2005
Available online 6 June 2005

Abstract

A detailed electrochemical study of a novel composite film based on ferrocene intercalated vanadium pentoxide xerogel/polyvinyl alcohol ($FeCp_2$/VXG–PVA–SbQ) and its potential use in the development of amperometric biosensors is presented. $FeCp_2$–VXG was characterized with X-ray powder diffraction, Mössbauer spectroscopy, energy dispersive spectroscopy and IR-spectroscopy suggesting a molecular formula close to $(FeCp_2)_{0.37} \cdot V_2O_5 \cdot nH_2O$. Composite films of $(FeCp_2)_{0.37} \cdot V_2O_5 \cdot nH_2O$ with PVA–SbQ were developed over a glassy carbon electrode. Cyclic voltammetry experiments showed that composite films exhibit reversible, almost charge-transfer controlled redox functions. The influence of various buffering systems composition on the working stability of the so modified electrodes was also investigated. Redox films were further modified by immobilizing glucose oxidase as a model enzyme. A remarkable electrocatalytic effect of the intercalated $FeCp_2$ towards the reduced form of the enzyme cofactor ($FADH_2$) was observed. Under optimized conditions, glucose biosensor was mounted into a flow injection analysis manifold and found to yield a linear response up to 10 mM glucose.

Keywords: Vanadium pentoxide xerogel; Ferrocene; Intercalation; Amperometric glucose amperometric biosensor; Photocrosslinkable styrylpyridinium modified polyvinyl alcohol

1. Introduction

Sol–gel-based biosensors have attracted enormous scientific attention, and a plethora of articles, dealing with the construction of biosensors based on sol–gel matrices, have been published [1–14]. Despite the volume of the published work, inherent drawbacks associated with the nature and the synthetic routes followed for the preparation of such gels still exist. These include cracking of the films, high concentration of methanol/ethanol in the resulted sol, and the most important point regarding the development of amperometric-based biosensors, the lack of conductivity. Grafting copolymers [15], addition of hydrophilic components [12,16], the use of sodium silicate as a precursor [17], and removal of the ethanol through the application of rotavapor methods [18] have been reported so far, as remedies to aforesaid drawbacks.

Inherently, redox intercalated vanadium pentoxide xerogels do not bear these disadvantages since they are

* Corresponding author. Tel.: +30 26510 98301; fax: +30 26510 98796.
E-mail addresses: ptrikal@chemistry.uoc.gr (P.N. Trikalitis), mprodrom@cc.uoi.gr (M.I. Prodromidis).

1388-2481/$ - see front matter © 2005 Elsevier B.V. All rights reserved.
doi:10.1016/j.elecom.2005.04.031

relatively conductive and no organic solvent is produced during their preparation. Vanadium pentoxide gels have a versatile lamellar structure which can intercalate a wide variety of inorganic and organic guest species and they exhibit electronic properties arising from electron hopping through the mixed-valence oxide network as well as ionic properties arising from proton diffusion in the aqueous phase [19–27].

This work reports for the first time on the electrochemical behavior of a composite film based on ferrocene intercalated $V_2O_5 \cdot nH_2O$ xerogel/PVA–SbQ. PVA–SbQ has been extensively used as a matrix for the immobilization of proteins [28–32]. The hydrophilicity of the polymer matrix, the mild conditions that are used during the immobilization and photopolymerization procedure make PVA–SbQ an effective support material for the immobilization of proteins.

Ferrocene intercalated $V_2O_5 \cdot nH_2O$ xerogel was also characterised by various physicochemical techniques. Using glucose oxidase as a model enzyme, prospects of GOx–PVA–SbQ/$FeCp_2$–VXG modified electrodes for further biosensor work in terms of working stability and storage stability, dynamic range, compatibility to proteins, applicability to near neutral pH, permeability and electrocatalytic activity were evaluated.

2. Experimental

2.1. Chemicals

Ferrocene was obtained from Fluka (Switzerland). Photocrosslinkable polyvinyl alcohol with styrylpyridinium residues (PVA–SbQ), was purchased from Toyo Gosei Kogyo (Japan). Glucose oxidase Type X-S (GOx, EC 1.1.3.4, from *Aspergillus niger*), D(+)-glucose, 2-[4-(2-hydroxyethyl)-1-piperazino]-ethanesulfonic acid (HEPES), 3-(*N*-morpholino)propane sulfonic acid (MOPS), Tris base, vanadium oxide, were obtained from Sigma (USA). Isopore polycarbonate membranes (porosity 0.1 μm, thickness 10 μm) were purchased from Millipore (USA). De-aerated double distilled water (DDW) was used throughout. A stock solution of glucose (0.2 M in DDW) was prepared 24 h before use.

2.2. Apparatus

For the electrochemical experiments a computer-controlled potentiostat, Autolab12 (EcoChemie, The Netherlands) was used. Cyclic voltammetry and chronocoulometry were performed in a three-electrode voltammetry cell using a glassy carbon electrode (3 mm diameter, BAS) as the working electrode, a Ag/AgCl/3 M KCl (BAS) reference electrode, and a Pt wire as auxiliary electrode. Flow measurements were carried out using an in-house fully automated FI manifold [33]. Energy dispersive spectroscopy (EDS) analysis was performed using an ISIS-300 microanalysis system by Oxford Instruments in combination with a JEOL JSM-5600 scanning electron microscope. FTIR spectra were recorded using a Perkin–Elmer (USA) spectrometer. ^{57}Fe Mössbauer spectra were recorded on a conventional constant acceleration spectrometer with a ^{57}Co(Rh) source. X-ray powder diffraction (Cu Kα radiation, $\lambda = 1.5418$ Å) was performed with a Brüker D8 advance in the range $5° < 2\theta < 50°$ with a resolution of 0.02° (2θ).

2.3. Preparation of $(FeCp_2)_{0.37} \cdot V_2O_5 \cdot nH_2O$ powder ($FeCp_2$–VXG)

$V_2O_5 \cdot nH_2O$ xerogel was prepared according to previous described procedure [27]. 0.266 g (1.43 mmol) $FeCp_2$ was dissolved in 75 mL acetonitrile, followed by addition of 0.5 g (2.38 mmol) of V_2O_5 xerogel. The mixture was incubated for 48 h at 60 °C. The product (a green-blue powder) was isolated by filtration through a Gooch 3 crucible, washed thoroughly with acetonitrile and allow to air-dry overnight.

2.4. Casting of PVA–SbQ/$FeCp_2$–VXG composite films and electrode assembly

An amount of 1 g PVA–SbQ polymer was diluted with 2.0 mL of DDW (50% w/v), followed by addition of 10 mg $FeCp_2$–VXG. The mixture was sonicated for 5 min and then left to become homogenous under strong agitation overnight. Correspondingly a mixture of 0.5 g PVA–SbQ with 2.0 mL DDW is defined as 25% w/v. A portion of 10 μL of the mixture (the mixture is not perfectly homogenous) was pipetted onto the surface of the electrode and spin-coated at 1500 rpm for 2 min. The film was then left to air-dry overnight (thickness ≈20 μm). Before use, modified electrodes were exposed to UV irradiation (wavelength 365 nm) for 1 h. Over the composite film a polycarbonate membrane was fitted with the aid of an O-ring.

2.5. Preparation of GOx–PVA–SbQ/$FeCp_2$–VXG composite films

An aliquot of the enzymic solution (100 U GOx in 5 μL 50 mM phosphate buffer pH 7) was added to 20 μL of PVA–SbQ/$FeCp_2$–VXG mixture and gently mixed. A portion of 5 μL of this mixture was spotted onto the surface of a glassy carbon electrode, spin coated at 1500 rpm for 2 min and left to dry overnight at +4 °C (thickness ≈20 μm). The film was then irradiated and covered with a polycarbonate membrane, as described above. Composite films were finally covered with a polycarbonate membrane.

3. Results and discussion

3.1. Characterization of vanadium oxide xerogel/ferrocene composite

The XRD pattern of $FeCp_2$–VXG and that of pristine $V_2O_5 \cdot nH_2O$ ($n \sim 1.6$) xerogel for comparison, are shown in Fig. 1. The pattern of $FeCp_2$–VXG shows a series of relatively broad Bragg peaks which have d spacings of the type d_{00l}/l ($l = 1$–7) and clearly indicates the lamellar structure of the material. These results show that the layer structure of pristine $V_2O_5 \cdot nH_2O$ xerogel is preserved during the reaction with ferrocene. Moreover, the (00 1) reflection, which corresponds to the interlayer distance is shifted towards lower 2θ values in the intercalated product indicating an expansion of the vanadium oxide layers. These results are summarized in Table 1 and are in full agreement with previous report [34].

The nature of iron in $FeCp_2$–VXG was investigated using ^{57}Fe Mössbauer spectroscopy. The spectrum of $FeCp_2$–VXG consists of a narrow singlet (68% relative area) that is typical for ferricinium cations [35–37], see Fig. 2 and Table 2. This result in combination with XRD data indicates that the intercalation of ferrocene molecules between the layers of $V_2O_5 \cdot nH_2O$ xerogel is a redox topotactic process during of which Fe(II) in ferrocene is oxidized to Fe(III) forming ferricinium ions [$(FeCp_2)^+$], while vanadium(V) in oxidic layers are partially reduce to V(IV). The partial reduction of V(V) to V(IV) in this system has been probed previously by ESR spectroscopy [34]. A tentative schematic representation of the atomic structure in $FeCp_2$–VXG is shown in Scheme I. The ^{57}Fe Mössbauer spectrum of $FeCp_2$–VXG contains also a doublet of Fe^{3+} (32% relative area) that could be assigned to distorted ferricinium ions (see Table 2). Although more experiments are necessary to clearly identify the nature of these species it is reasonable to expect some distortions from the ideal structure of ferricinium ions being in such a confined environment. The V:Fe atomic ratio was determined by EDS, suggesting a molecular formula close to $(FeCp_2)_{0.37} \cdot V_2O_5 \cdot nH_2O$.

The structural integrity of the vanadium oxide layered framework after redox intercalation reaction with ferrocene was also confirmed by IR spectroscopy. The corresponding FTIR spectra (data not shown) show

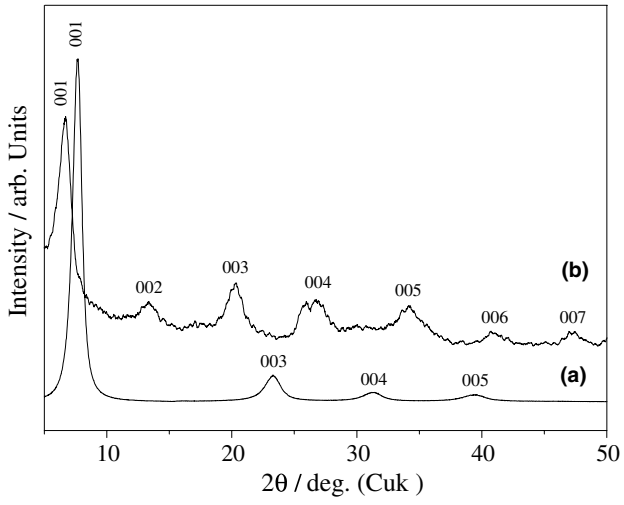

Fig. 1. X-ray powder pattern of: (a) pristine $V_2O_5 \cdot nH_2O$; (b) $FeCp_2$–VXG intercalated product.

Table 1
Interplanar d spacings of observed Bragg peaks for pristine and intercalated materials derived from powder XRD data

Material	d_{001}	d_{002}	d_{003}	d_{004}	d_{005}	d_{006}	d_{007}
$V_2O_5 \cdot nH_2O$	11.5		3.8	2.9	2.3		
$FeCp_2$–VXG	13.2	6.6	4.4	3.4	2.6	2.2	1.9

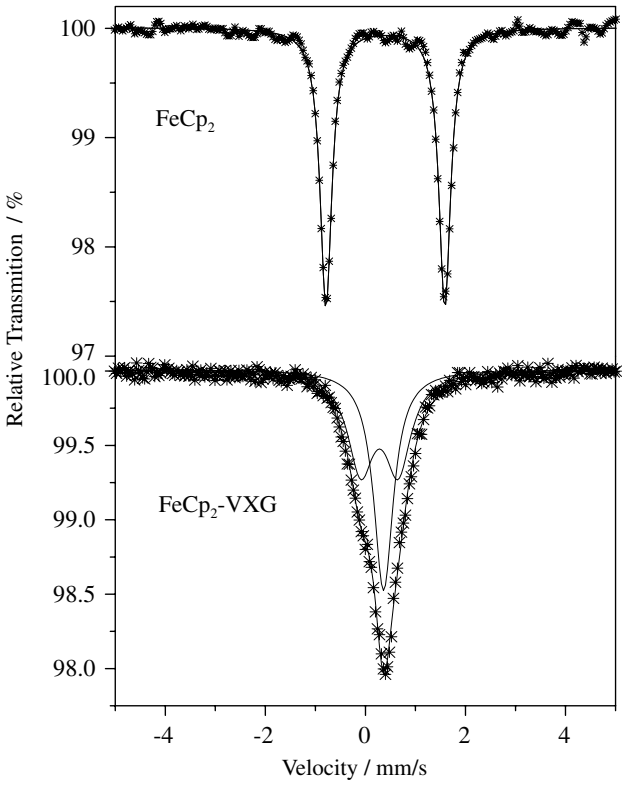

Fig. 2. ^{57}Fe Mössbauer spectra of ferrocene and $FeCp_2$–VXG.

Table 2
^{57}Fe Mössbauer data for ferrocene and intercalated material

Material	IS	ΔE_p	Area (%)
$FeCp_2$	0.50	2.37	100
$FeCp_2$–VXG	0.47	0	68
	0.41	1.06	32

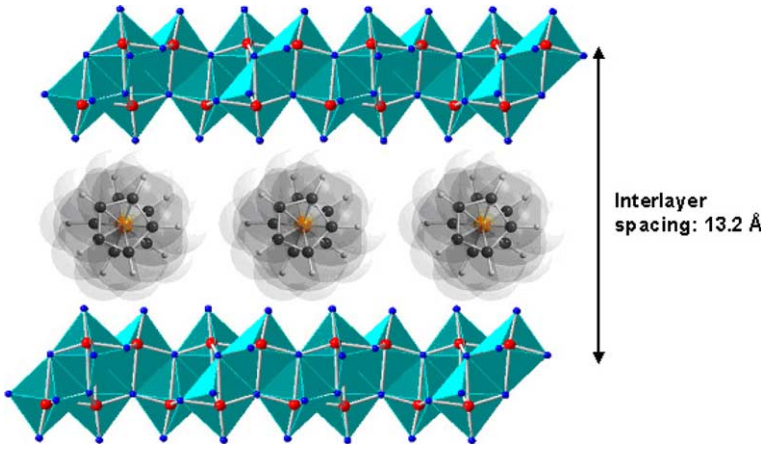

Scheme I. Ferricinium ions intercalated between V_2O_5 layers in $FeCp_2$–VXG material.

three characteristic vibration bands from the V_2O_5 framework below 1100 cm^{-1}. The band at ~1000 cm^{-1} is assigned to the V=O stretching vibration and the bands at ~750 and ~500 cm^{-1} are attributed to the in-plane and out-of-plane V–O–V vibrations, respectively [38]. The presence of the three bands suggests that the reduced V_2O_5 framework is structurally intact with respect to the pristine $V_2O_5 \cdot nH_2O$ framework.

3.2. Electrochemistry of the $FeCp_2$ intercalated V_2O_5 xerogel

The synthetic procedure of ferrocene intercalated solid $(FeCp_2)_x \cdot V_2O_5 \cdot nH_2O$ was optimized based on the electrochemical characteristics of the final composite material. Using various $FeCp_2 \cdot V_2O_5 \cdot nH_2O$ molar ratio in the range 0.3–1.0 the optimum CV grams pattern was recorded for the solid with formula $(FeCp_2)_{0.37} \cdot V_2O_5 \cdot nH_2O$.

Despite the well-known vanadium pentoxide redox properties [39,40], flat CVs were obtained for a PVA–SbQ–VXG modified electrode in 50 mM phosphate or Tris buffer solutions at pH 7. The absence of defined peaks could be explained by electrolyte migration and reorganization of redox sites in the composite film, which lead to a stationary condition [20,41].

The insets of Fig. 3 shows cyclic voltammograms of PVA–SbQ/$FeCp_2$–VXG films in 50 mM Tris buffer solution at pH 7, at various scan rates. Plots of the anodic and cathodic peak currents for the reduction and oxidation of the intercalated ferrocene/ferricinium couple vs. the potential scan rate, v, were nearly linear from 0.01 to 0.4 $V s^{-1}$ (Fig. 3(a)), suggesting facile charge transfer kinetics over this range of sweep rates as expected for intercalated ferrocene molecules [42]. At faster scan rates, however, from 0.6 to 10 $V s^{-1}$ the relationship becomes linear only when current values plotted vs. the square root of v (Fig. 3(b)) indicating mass transport limited within the film. This is specifically true in a regime of high surface coverage, as it happens in case of ferrocene intercalated V_2O_5 xerogel lamellae, and high sweep rates. Under these high sweep rates the diffusion step dominates the procedure. The diffusion mechanism

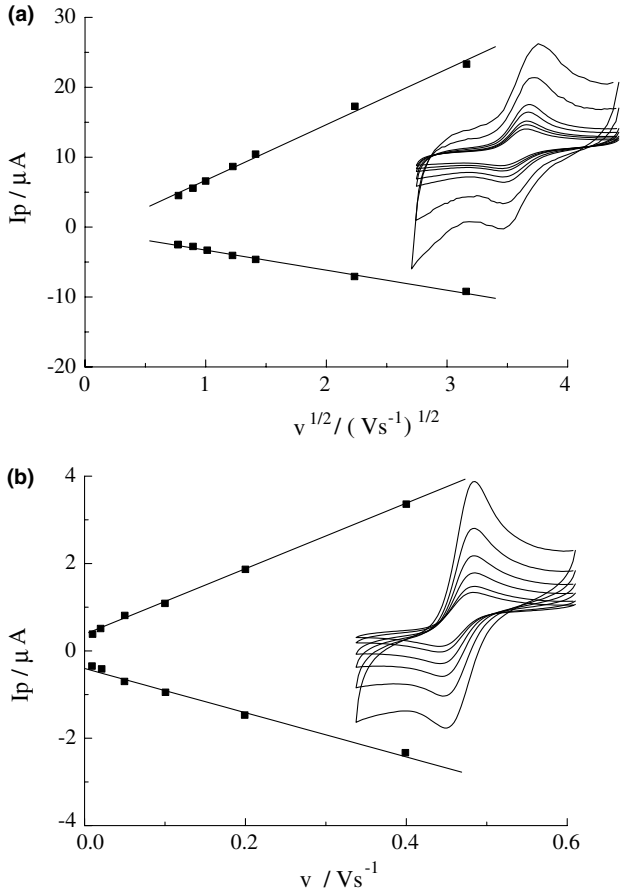

Fig. 3. Variation of I_p with (a) the square root of scan rate and (b) the scan rate for the PVA–SbQ/$FeCp_2$–VXG. Inset: Cyclic voltammograms represent the experimental data for scan rates: (a) 0.6, 0.8, 1, 1.5, 2, 5, 10 $V s^{-1}$; (b) 0.01, 0.02, 0.05, 0.1, 0.2, 0.4 $V s^{-1}$. Buffer solution: 50 mM Tris, pH 7.

is presumably attributable to electron transfer (hopping) among the mediator redox centres as well as between the latter and the $V_2O_5 \cdot H_2O$ ($V^{4+} \leftrightarrow V^{5+}$) framework. Is mostly unlikely the actual physical diffusion of the ferrocene moieties within the $V_2O_5 \cdot H_2O$ lamellae.

The separation between the anodic and cathodic peak potentials, ΔE_p, values for scan rates 0.01–0.4 $V s^{-1}$ moderate between 48 and 55 mV, while for scan rates 0.4–2 $V s^{-1}$ the ΔE_p varies between 58 and 73 mV. The observed non-ideal electrochemical behavior of the intercalated mediator can mainly be attributed to strong interactions between intercalated molecules and the surface structural heterogeneity of the film.

The (apparent) electron transfer rate constants k^o were calculated from Tafel diagrams [42], and mean values of $k_a^o = 36 \pm 10\ s^{-1}$ and $k_c^o = 28 \pm 8\ s^{-1}$ were calculated by applying equation $k^o = 2.303anFv_o/RT$. However, it is lower compared to $k_a^o = 54 \pm 22\ s^{-1}$ and $k_c^o = 58 \pm 25\ s^{-1}$ values are reported for the ferrocene covalently attached to platinum surface [43], suggesting a slower electron kinetics probably due to the polymeric environment of the intercalated ferrocene.

3.3. Stability of the electrochemical sensor

The stability of PVA–SbQ/$FeCp_2$–VXG sensor was studied by monitoring the (redox) activity (Fig. 4) of it during 1000 successive sweeps (potential ranges between +0.6 and −0.1 V) in different buffering systems. As it can be seen in Fig. 4 the stability of the sensor was very poor in the phosphate buffer solution, which has Na^+ (or K^+) as counter ions. This behavior can be understood on the basis of an ion-exchange process between $FeCp_2$ and the

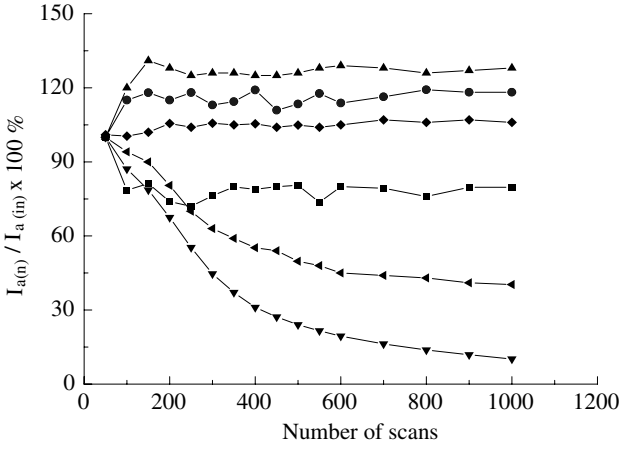

Fig. 4. Stability of the PVA–SbQ/$FeCp_2$–VXG in different 50 mM buffer solutions at pH 7: (■) MOPS (●) HEPES, (▲) Tris, (▼) Phosphate; (□) PVA–SbQ/$FeCp_2$ electrode in 50 mM phosphate pH 7 buffer solution; (◀) PVA–SbQ/$FeCp_2$–VXG (not protected by an outer polycarbonate membrane) in 50 mM MOPS buffer solution, pH 7. The stability of PVA–SbQ/$FeCp_2$–VXG electrodes is estimated by the current response of each cycle divided by the current response of the 50th scan × 100%.

Na^+ or K^+ cations resulting in the de-intercalation of the former from the interlayer space of the vanadium xerogel host material. This process would result in material with reduced amount of $FeCp_2$ and poor electrochemical stability [22,40]. In order to minimize this process, buffering systems based on relatively bulk organic molecules, that is, MOPS, HEPES and Tris buffers (pH adjustment was made with triethylamine in the former two and trizma HCl in the latter) were employed. A remarkable stability was achieved in the presence of these buffering systems, thus allowing the use of the proposed electroactive film in analytical applications.

The behavior of the system in the presence of the above-mentioned buffering systems shows that the stability of the proposed architectures is strongly related with (among the others parameters, that is, charge and hydrophobicity) the relative size of the counter ions of the electrolyte. Probably, based on a size-exclusion mechanism, MOPS, HEPES and Tris molecules do not provoke ion exchange of ferrocene molecule from the $V_2O_5 \cdot H_2O$ framework.

A PVA–SbQ/$FeCp_2$ electrode was also constructed and the same stability test was run as a control experiment. As it can be seen in Fig. 4, PVA–SbQ/$FeCp_2$ electrodes also appeared a remarkable stability; however, recorded currents were considerable lower (ca. 20%) compare with those recorded in PVA–SbQ/$FeCp_2$–VXG films (data not shown). This difference can be attributed to V_2O_5 xerogel, which serves as an electron-transfer mediator, shuttling electrons between the electrode surface and the redox centers within the V_2O_5 framework, reinforcing thus the electrochemical properties of the intercalated moieties. The stability curves of PVA–SbQ/$FeCp_2$–VXG films in both HEPES and Tris buffer solutions have a characteristic pattern; both of the anodic and cathodic currents are increased during the course of the first scans (conditioning period in the working electrolyte), leveling at a maximum value after 150–200 scans.

3.4. Electrocatalytic oxidation of glucose

Fig. 5 shows cyclic voltammograms obtained with GOx–PVA–SbQ/$FeCp_2$–VXG biosensors in the presence of two different concentrations of glucose at pH 7. A large catalytic current flows at oxidizing potentials. This behavior is indicative of the regeneration of ferrocene from the ferricinium ion by the reduced form of the GOx coenzyme (FAD-H_2) at the potential where ferricinium ion ($E^{o'} = 204$ mV) dominates, compared with the current recorded at the same potential in the absence of glucose. This behavior indicates a strong electrocatalytic effect and can be interpreted as follows: glucose present in the solution diffuses through the film and reduces the GOx coenzyme (Scheme II). The reduced form of the coenzyme (FAD-H_2) is then oxidized by the

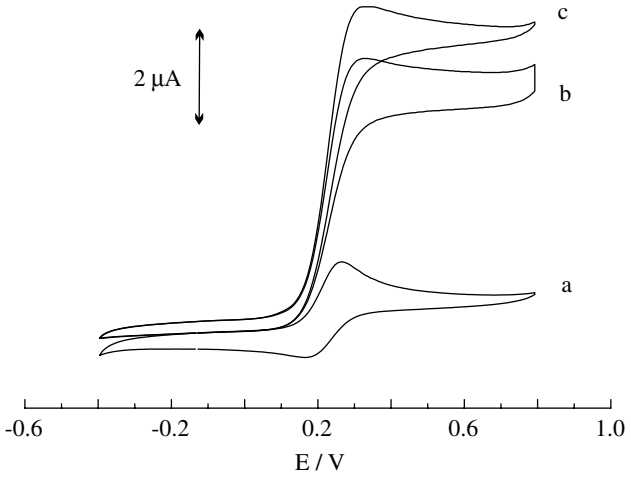

Fig. 5. Cyclic voltammograms illustrating the catalytic oxidation of glucose mediated by GOx–PVA–SbQ/$FeCp_2$–VXG modified electrodes (a): CV of GOx–PVA–SbQ/$FeCp_2$–VXG in the buffer solution, (b) CV of the same GOx–PVA–SbQ/$FeCp_2$–VXG in the buffer solution containing 4 mM glucose and (c) 5 mM glucose. Scan rate: 10 $mV\,s^{-1}$. Buffer solution: 50 mM Tris, pH 7.

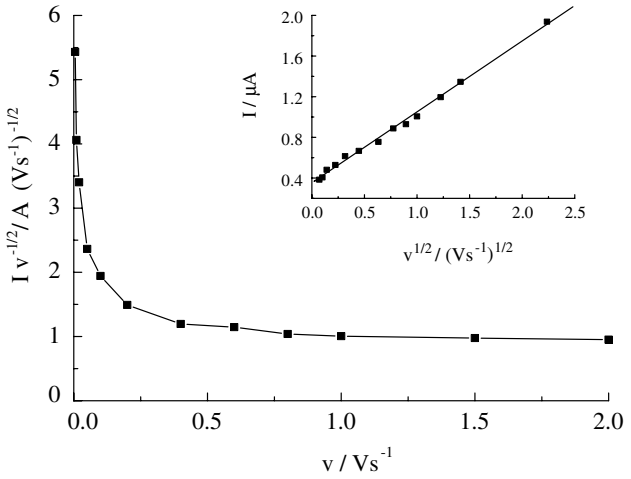

Fig. 6. Variation of the sweep rate-normalized current with the sweep rate for PVA/Fc-VXG/GOx modified electrodes in the presence of 4 mM glucose. Inset: variation of I_{pa} with the square root of the scan rate for the GOx–PVA–SbQ/$FeCp_2$–VXG modified electrodes in the presence of 4 mM glucose. Buffer: 50 mM Tris, pH 7.

ferricinium ions present in the film, and the latter is reducing to ferrocene, which then is electrochemically oxidized to ferricinium ions at potential >+0.2 V. This catalytic cycle gives rise in a large increase in the anodic current and a corresponding decrease in the accompanying reduction in the cathodic region. The anodic current increases proportionally to the concentration of glucose concentration. The plot (Fig. 6, inset) of the catalytic peak current (corrected to the baseline) is linearly increased with the square root of the sweep rate suggesting, that at sufficient overpotential the reaction is mass-transferred limited.

A current measurement-based diagnostic test was utilized for the identification of the mechanism illustrated in Scheme II [44]. A catalytic regeneration mechanism (variation of the EC mechanism) was justified by the shape of the plot of the sweep rate-normalized current ($i/v^{1/2}$) vs. sweep rate. The peak current function for this reaction obeys the prediction for this type of mechanism, it is large at low scan rates and decreases to a constant value at higher scan rates as shown in Fig. 6. This diagnostic experiment in combination with the large catalytic (anodic) currents in Fig. 5, are strong evidences that the enzymatic oxidation of glucose is proceeding through the proposed mechanism (Scheme II) and not through the oxidation of the enzymatically produced hydrogen peroxide. The latter is dominated in oxygenated buffer solution and under sufficient overpotentials (>0.65 V) in the absence of a mediator for FAD-H_2 oxidation [45].

The (apparent) electrochemical rate constant of the reaction between glucose and the intercalated mediator was graphically calculated [42] 2.2×10^4 and 3.8×10^4 $M^{-1}s^{-1}$ for GOx–PVA–SbQ/$FeCp_2$–VXG biosensors constructed from PVA–SbQ solutions of 50% and 25%, respectively. The diffusion coefficient of glucose under specific experimental conditions was calculated by double step chronocoulometry [42] and was found 3.68×10^{-10} and 6.77×10^{-10} cm^2s^{-1} for GOx–PVA–SbQ/$FeCp_2$–VXG biosensors constructed from PVA–SbQ solutions 50% and 25%, respectively.

3.5. Optimization of the film composition

GOx–PVA–SbQ/$FeCp_2$–VXG biosensors were mounted on a flow-through amperometric cell and

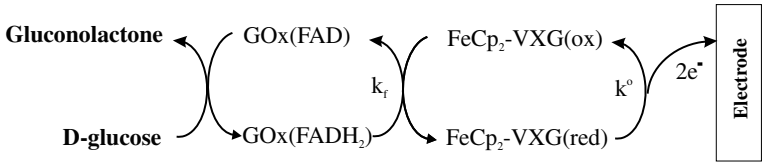

Scheme II. Regeneration of the $FeCp_2$–VXG following the catalytic EC mechanism and current flow through the coupling enzymatic reaction of GOx regenerated. k^o is the electron transfer rate constant of the of ferrocene/ferricinium redox couple within the film and k_f the electrochemical rate constant for the catalytic oxidation of glucose present in the solution.

the performance of the system was investigated for different enzyme loadings (25, 50, 75, 100 U GOx) and two different concentrations of PVA–SbQ (50% and 25% w/v at the optimum enzyme content). The composition of the membrane was as follows: (U×) GOx – 50% w/v PVA–SbQ/10 mg $FeCp_2$–VXG. The relative apparent measurable efficiencies with respect to the highest peak current were: 53%, 74%, 100% and 100%, respectively. The effect of the concentration of PVA–SbQ on the performance of the system was evaluated with membranes of the following composition, (100 U) GOx–(25% and 50% w/v) PVA–SbQ/ 10 mg $FeCp_2$–VXG, taking as criterion the linearity of the system over glucose concentration.

As it can be seen in Fig. 7, the concentration of the polymer in the composite film is a key parameter for the analytical performance of it. Composite biofilms made from 25% w/v PVA–SbQ are linear over the concentration range 0.1–10 mM glucose, whereas PVA–SbQ concentrated films exhibit a sigmoid response with a restricted linearity (2–10 mM glucose). Restriction of the glucose flux through the denser composite films and steric hindrance of the enzyme resulting to insufficient interaction with its substrate or partial inactivation of some of the GOx active centers can explain the low sensitivity of the system at concentrations <2 mM glucose.

Throughout this study the concentration of $FeCp_2$–VXG in the film was kept constant at 10 mg $FeCp_2$–VXG in 2 mL PVA–SbQ 50% or 25% w/v. Lower amounts of $FeCp_2$–VXG gave accordingly lower response, whereas higher amounts result to a sticky mixture with no practical use as regards the casting of the film.

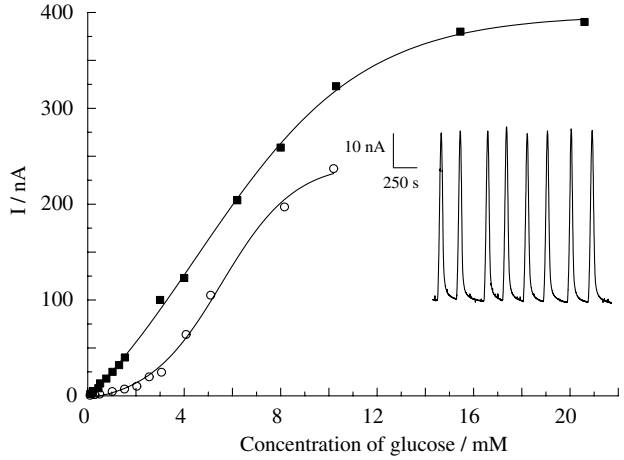

Fig. 7. Calibration curves of glucose with (■) 25% w/v, (○) 50% w/v GOx–PVA–SbQ/$FeCp_2$–VXG biosensors. Inset graph; reproducibility of the system (1.5 mM glucose, $n = 8$). FI traces were recorded with a 25% w/v GOx–PVA–SbQ/$FeCp_2$–VXG-based biosensor under optimum conditions.

3.6. Analytical performance

From the results obtained during the stability study of the proposed biosensors, is obvious that one of the most popular buffering systems, that is, phosphate buffer, should be excluded. However, the rest of the tested buffers should be no considered as a special condition, since they are also among the most widely used buffers in bioanalytical applications. The performance of GOx–PVA–SbQ/$FeCp_2$–VXG biosensors was studied in Tris buffer over the pH range 6–9; higher sensitivity was obtained at pH 8. Due to the acidic behavior of the V_2O_5 framework [24] this value is slightly higher compared with optimum pH values have been reported for immobilized GOx [45].

Linear parts for the tested configurations (25 and 50% w/v PVA–SbQ) are fitting the equations, current (nA) = −2.8 + 32.6 [glucose] (mM), $r^2 = 0.9975$ (Fig. 7) and current (nA) = −5.7 + 29.8 [glucose] (mM), $r^2 = 0.9901$, respectively. Limit of detections, for a signal-to-noise ratio of 3, were calculated 0.05 and 1 mM glucose, respectively. The relative standard deviation (RSD) of the method for the 25% w/v PVA–SbQ-based films was calculated as 1.8% ($n = 8$, 1.5 mM glucose) (Fig. 7, inset).

Membranes retain almost 95% of their original activity after 120–150 analytical runs. We tried unsuccessfully to extend the working stability of the membranes increasing the enzyme loadings at 150 U GOx. At these loadings the resulted membranes were not uniform; this phenomenon can be attributed to the phase separation of the photocrosslinkable polymer and the protein during the drying process of the polymer layer [32]. When not in use, biosensors were stored dry at +4 °C retain almost 85% of their initial activity after a period of three weeks.

4. Conclusions

Ferrocene intercalated vanadium pentoxide xerogel/ polyvinyl alcohol composite film was tested for first time as an electrocatalyst and host protein platform to develop an amperometric biosensor. The proposed films exhibit a reversible redox behavior and offer a low-potential detection of FAD-H_2. Compare with other xerogel-based architectures, vanadium pentoxide xerogel is superior in terms of conductivity and compatibility to enzymes. The proposed electrocatalyst provides about 20% increase of the sensitivity compared with the pure mediator, is compatible with biomolecules and its applicability over the useful pH range for most of the (bio)sensors applications indicates promise for further use. However, the observed instability in the presence of small cations prevents the direct use of the proposed films in undiluted real samples. To overcome this

problem, overlay of the proposed composite films with charge repulsing coatings is currently under investigation in our laboratory.

References

[1] S. Braun, S. Rappoport, R. Zusman, D. Avnir, M. Ottolenghi, Mater. Lett. 10 (1990) 1.
[2] L.M. Ellerby, C.R. Nishida, F. Nishida, S.A. Yamanaka, B. Dunn, J.S. Valentine, J.I. Zink, Science 255 (1992) 1113.
[3] P. Audebert, C. Demaille, C. Sanchez, Chem. Mater. 5 (1993) 911.
[4] S.S. Rosatto, P.T. Sotomayor, L.T. Kubota, Y. Gushikem, Electrochim. Acta 47 (2002) 4451.
[5] F. Gelman, J. Blum, D. Avnir, J. Am. Chem. Soc. 124 (2002) 14460.
[6] J. Wang, P.V.A. Pamidi, D. Su Park, Anal. Chem. 68 (1996) 2705.
[7] E.J. Cho, Z. Tao, E.C. Tehan, F.V. Bright, Anal. Chem. 74 (2002) 6177.
[8] A. Kumar, R. Malhotra, B.D. Malhotra, S.K. Grover, Anal. Chim. Acta 414 (2000) 43.
[9] I. Gill, Chem. Mater. 13 (2001) 3404.
[10] W. Jin, J.D. Brennan, Anal. Chim. Acta 461 (2002) 1.
[11] S. Cosnier, A. Senillou, M. Gratzel, P. Comte, N. Vlachopoulos, N.-J. Renault, C. Martelet, J. Electroanal. Chem. 469 (1999) 176.
[12] B. Prieto-Simon, G. Armatas, Ph.J. Pomonis, C.G. Nanos, M.I. Prodromidis, Chem. Mater. 16 (2004) 1026.
[13] P.B. Gaspers, A.P. Gast, C.R. Robertson, J. Colloid Interf. Sci. 172 (1995) 518.
[14] D. Advir, Acc. Chem. Res. 28 (1995) 328.
[15] B. Wang, J. Zhang, S. Dong, Biosens. Bioelectron. 15 (2000) 397.
[16] S. Sampath, O. Lev, Electroanalysis 8 (1996) 1112.
[17] M.L. Ferrer, F. del Monte, D. Levy, Chem. Mater. 14 (2002) 3619.
[18] R.B. Bhatia, C.J. Brinker, Chem. Mater. 12 (2002) 2434.
[19] M.A. Fox, M.T. Dulay, Chem. Rev. 93 (1993) 341.
[20] F.J. Anaissi, G.J.-F. Demets, H.E. Toma, A.C.V. Coelho, J. Electroanal. Chem. 464 (1999) 48.
[21] E.C. Zampronio, D.N. Greggio, H.P. Oliveira, J. Non-Cryst. Solids 332 (2003) 249.
[22] G.N. Barbarosa, T.A.F. Lassali, H.P. Oliveira, Solid-State Ionics 169 (2004) 15.
[23] V. Glezer, O. Lev, J. Am. Chem. Soc. 115 (1993) 2533.
[24] J. Livage, Chem. Mater. 3 (1991) 578.
[25] V. Petkov, P.N. Trikalitis, E.S. Bozin, S.J.L. Billinge, T. Vogt, M.G. Kanatzidis, J. Am. Chem. Soc. 124 (2002) 10157.
[26] M.G. Kanatzidis, C.G. Wu, H.O. Marcy, C.R. Kannewurf, J. Am. Chem. Soc. 111 (1989) 4139.
[27] P.N. Trikalitis, V. Petkov, M.G. Kanatzidis, Chem. Mater. 15 (2003) 3337.
[28] A.P. Soldatkin, J. Montoriol, W. Sant, C. Martelet, N. Jaffrezic-Renault, Mat. Sci. Eng. C 21 (2002) 75.
[29] A. Silvana, L. Barthelmebs, J.-L. Marty, Anal. Chim. Acta 464 (2002) 171.
[30] K.S. Chang, W.L. Hsu, H.Y. Chen, C.K. Chang, C.Y. Chen, Anal. Chim. Acta 481 (2003) 199.
[31] F. Mizutani, T. Sawaguchi, Y. Sato, S. Yabuki, S. Iijima, Anal. Chem. 73 (2001) 5738.
[32] C.G. Tsiafoulis, M.I. Prodromidis, M.I. Karayannis, Biosen. Bioelectron. 20 (2004) 620.
[33] M.I. Prodromidis, A.B. Tsibiris, M.I. Karayannis, J. Autom. Chem. 17 (1995) 187.
[34] S. Okuno, G. Matsubayashi, Bull. Chem. Soc. Jpn. 66 (1993) 459.
[35] J.S. Miller, J.H. Zhang, W.M. Reiff, J. Am. Chem. Soc. 109 (1987) 109.
[36] P.S. Bagus, U.I. Walgren, J. Almlof, J. Chem. Phys. 64 (1976) 2324.
[37] J.S. Miller, J.H. Zhang, W.M. Reiff, Inorg. Chem. 26 (1987) 600.
[38] L. Abello, E. Husson, Y. Repelin, G.J. Lucazeau, Solid-State Chem. 56 (1986) 379.
[39] H.P. Oliveira, C.F.O. Graeff, C.L.P. Zanta, A.C. Galina, P.J. Gonçalves, J. Mater. Chem. 10 (2000) 371.
[40] J. Livage, Solid-State Ionics 86–88 (1996) 935.
[41] L.F. Silva, L.P.R. Profeti, N.R. Stradiotto, H.P. Oliveira, J. Non-Cryst. Solids 298 (2002) 213.
[42] A.B. Florou, M.I. Prodromidis, S.M. Tzouwara-Karayanni, M.I. Karayannis, Electroanalysis 10 (1998) 1261.
[43] M. Sharp, M. Petersson, K.J. Edstrom, J. Electroanal. Chem. 95 (1979) 123.
[44] P.T. Kissinger, W.R. Heinmann (Eds.), Laboratory Techniques in Electroanalytical Chemistry, second ed., Marcel Dekker, Inc., New York, 1996.
[45] A.E.G. Cass, G. Davis, G.D. Francis, A.O. Hill, W.J. Aston, J. Higgins, E.V. Plotkin, L.D.L. Scott, A.P.F. Turner, Anal. Chem. 58 (1984) 667.